Importance of spectrally invariant broadband attenuation of light in indoor photovoltaic characterization

Stefan Zeiske ✉ 🆔 ; Paul Meredith 🆔 ; Ardalan Armin 🆔 ; Gregory Burwell ✉ 🆔

Check for updates

View Online   Export Citation

Articles You May Be Interested In

Performance measurements for indoor photovoltaic devices: Classification of a novel light source

APL Energy (March 2024)

Comprehensive study of microcrystalline silicon solar cells deposited at high rate using 13.56 MHz plasma-enhanced chemical vapor deposition

J. Vac. Sci. Technol. A (March 2002)

Micro-pixelated halide perovskite photodiodes fabricated with ultraviolet laser scribing

Appl. Phys. Lett. (May 2024)

AIP Publishing

Special Topics Open for Submissions

Learn More

AIP Publishing

Importance of spectrally invariant broadband attenuation of light in indoor photovoltaic characterization

View Online   Export Citation   CrossMark

Stefan Zeiske,[a)] 🆔 Paul Meredith, 🆔 Ardalan Armin, 🆔 and Gregory Burwell[a)] 🆔

AFFILIATIONS

Sustainable Advanced Materials (Sêr-SAM), Department of Physics, Swansea University, Singleton Park, Swansea SA2 8PP, United Kingdom

[a)]Authors to whom correspondence should be addressed: stefan.zeiske@swansea.ac.uk and g.burwell@swansea.ac.uk

ABSTRACT

Indoor photovoltaic (IPV) devices are poised to make a significant contribution to the proliferation of the "Internet of Things" (IoT). For the accurate intercomparison of IPVs (and, hence, to advance the rational development of the technology), lighting conditions representative of those in typical indoor settings must be created reproducibly. As indoor lighting is invariably broadband, this will typically require the use of optical attenuation to achieve varying irradiance conditions at the device under test location. However, most forms of optical attenuation will suffer from some degree of spectral dispersion, creating sources of uncertainty for key figures of merit, such as power conversion efficiency. In this work, we examine the contribution of the mode of optical attenuation to the accurate characterization of IPV systems. We discuss requirements for broadband light source attenuation for the accurate characterization of photovoltaic devices under indoor illumination and consider the importance of using suitable reference devices for light intensity calibration. Furthermore, we experimentally verify attenuation methods typically used, including power control of the light source itself, use of neutral density filters, and advanced attenuation based on tandem prism attenuators. Finally, spectral shape alteration-induced uncertainties in performance parameter determination of photovoltaic cells under indoor illumination are quantified for three common broadband light attenuation methods, where we found ~2%, ~6%, and up to ~15% ambiguity in photovoltaic device efficiency when using LED power control, prism attenuators, and neutral density filter-based broadband light attenuation, respectively.

INTRODUCTION

Over the past few years, indoor photovoltaic (IPV) technology has witnessed notable advancements in device efficiency and fabrication development.[1–5] As a result, IPV has emerged as a promising solution for powering Internet of Things (IoT) devices that are widely utilized in various fields such as electronics, sensing, and machine learning via the harvesting and utilization of ambient light.[3,5–8] Compared to outdoor photovoltaics, IPV technology presents fewer complexities thanks to the relatively lower light levels and gentler operating conditions typically encountered indoors. These favorable conditions contribute to enhanced device longevity, which opens up new possibilities for solution-processed semiconductors such as perovskites and organic materials.[8–13] The tunability of the energy bandgap of these materials and their low embodied energy make them particularly well-suited for IPV applications, thus driving further interest and exploration in this domain.

As new PV materials and devices are being developed for IPV use, the lack of standardized light sources (LSs) (in terms of both spectrum and irradiance) for IPV testing complicates their development as different loss mechanisms dominate at different intensities.[14,15] Real-world IPV devices operate under variable conditions, requiring benchmarking with a range of lighting conditions.[16] Accurate characterization of IPV devices is necessary for their development, with research focusing on experimental factors such as spectral validation, illumination masks, stray light, and radiation uniformity.[17,18] Subsequently, measuring IPV devices under a range of irradiances reflects real-world scenarios and helps to identify dominant power conversion efficiency (PCE) loss mechanisms essential for optimizing IPV development.[19]

Light intensity-dependent photocurrent (IPC) measurement has been previously reported as a powerful tool for understanding photovoltaic device fundamentals.[20,21] In particular, this experimental technique can identify different photocurrent loss mechanisms that are effective at different intensities. IPC provides insight into the varying performance-limiting factors, including trap-assisted recombination, bimolecular recombination, the build-up of space-charge due to imbalanced mobility of charge carriers, and series resistance limitations.[22] Experimentally, IPC measurements are typically conducted by varying the irradiance at a single wavelength over orders of magnitude. This can be achieved using a laser light source with variable output power in combination with an attenuator, for example, a series of neutral density (ND) filters, resulting in a quasi-continuum of points in the irradiance regime of interest. Prior to an IPC measurement, a photodiode of known responsivity is typically used as a reference device for light calibration. Similarly, the measurement of the open circuit voltage's (V_{oc}) dependence on irradiance can also yield insights into the operation of a PV system.[23,24] The IPC measurement technique discussed above, utilizing a laser light source with variable output power, offers a straightforward approach to investigating the light intensity dependence of photocurrent. However, it is important to note that this simple approach may not be as straightforward when working with broadband sources.

The characterization of device performance under various indoor illumination intensities is, in turn, complicated due to the tendency of most attenuation techniques to change the spectral shape of broadband light sources. Such an erratic phenomenon can affect the beam quality (i.e., beam homogeneity and spectral validation) and the linearity of the calibration.[25] While the latter will inevitably be linked to errors in light intensity determination using reference devices, the former will ultimately affect IPV cell and module performance characterization. Such links between attenuator-induced spectral effects of broadband light sources and related uncertainties in device PV parameters probed under indoor illumination have not been established yet but are of utmost importance for driving development and research in the IPV community—this was indeed the case in the development of outdoor PV standards.

In this work, we outline the importance of considering spectral-dependent effects when attenuating broadband light sources for IPV characterization. We experimentally verified the attenuation methods typically used. We further consider the importance of using suitable reference devices and demonstrate the need for spectrally stable light attenuation from broadband light sources for IPV device characterization. Following this, we determine the uncertainties in device PV parameters as associated with different broadband light source attenuation techniques.

RESULTS AND DISCUSSION

Optical attenuation of broadband light sources with constant radiant power

In general terms, the attenuation of a light source with constant radiant power can be achieved either by spatial means (similar to changing the aperture of a camera lens) or by the interaction of light with a medium (such as optical filters). In the former case, the irradiance at a point at some distance from a light source can be

modified by changing the distance between them. If the light source is point-like, this can be approximated by the inverse square law. However, as IPV cells or modules must have sufficient size to deliver the required input power, there must be sufficient spatial uniformity (H_f) across the device under test (DUT) location to measure the devices accurately. For a point source, this can be approximated as

$$H_f = \left(w^2\right)/\left(2d_1^2 + w^2\right)(\times 100\%),\qquad(1)$$

where w is the half-width of the device and d_1 is the distance to the point light source. A full derivation is provided in the supplementary material, Note 1. This method of attenuation is, therefore, the most straightforward in terms of experimental apparatus, and wavelength-dependent effects are minimal. However, its practicality is limited for reproducible IPV measurements, which require sufficient H_f across the DUT location.

In situations where large-area IPV devices are to be measured at typical indoor module scales ($\sim$30 cm^2), methods of optical attenuation involving the interaction of light with a medium are more practical. When light interacts with any medium, it can be either transmitted, reflected, or absorbed. This can be expressed as $T + R + A = 1$, where T, R, and A are the transmittance, reflectance, and absorptance, respectively, which are dependent on the wavelength λ. It can be convenient to describe the use of optical components using transfer matrices, for example,

$$M_{DUT} = M_1 \ldots M_N M_{Source},\qquad(2)$$

where M_{Source} describes the light source, M_{DUT} describes the DUT location, and $M_1 \ldots M_N$ are optical elements between them. The simplest optical element to consider is the ND filter. These are common optical components, which are described by their optical density (OD), defined by $T = 10^{-OD}$. In the case of an ideal ND filter used to attenuate a light source, this can be described as

$$M_{DUT} = M_{ND} M_{Source},\qquad(3)$$

where, in the ideal case, M_{ND} is the diagonal matrix with the transmittance of the filter T given by the above expression, which is constant at all wavelengths. However, no real ND filter has a constant T across the broadband visible spectrum. This is true for both reflective and absorptive ND filters, which will have some degree of dispersion across a broadband wavelength range. Figure 1(a) shows the normalized irradiance of an LED source plotted as a function of wavelength (detailed information on the measurement of the LED spectra and the conversion of the spectral photon flux to irradiance units is provided in the supplementary material, Notes 1 and 2). The transmittance of an ND filter is shown in Fig. 1(b). Finally, Fig. 1(c) shows the change in spectrum shape of the LED after ND filter attenuation (red solid line) as compared to before attenuation (black solid line). Noticeably, an ND filter-induced change in LED emission peak ratio (i.e., emission peaks at $\sim$300 nm and $\sim$400 nm) and a noticeable contribution of high wavelengths (i.e., >500 nm) are observed.

Another method of optical attenuation with a low degree of spectral dispersion is the use of arrays of micromirrors, such as those found in a digital micromirror device (DMD),[25] which can reflect the incident beam at varying angles. The irradiance at a given location
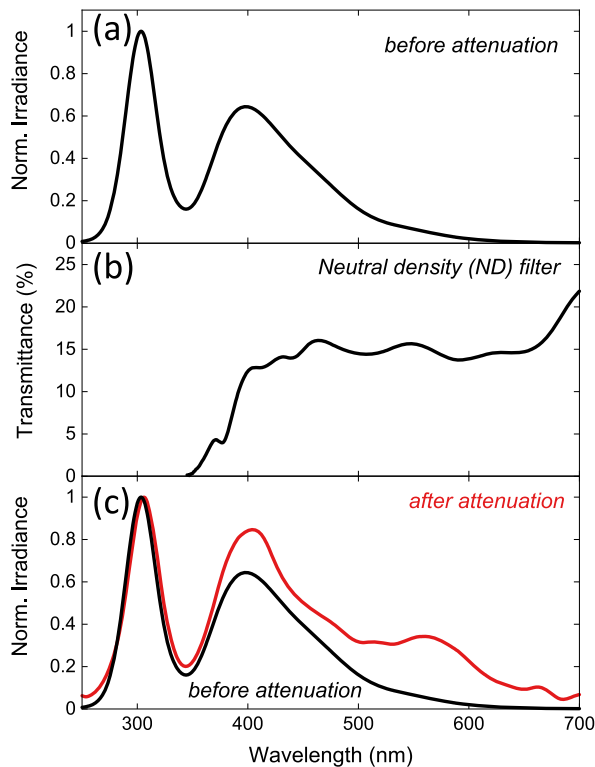
FIG. 1. Comparison of (a) the normalized spectral irradiance of an LED source before attenuation; (b) the transmission function of a neutral density filter (ND30B, Thorlabs) with an optical density (OD) of 3; and (c) the resultant spectrum after attenuation (red solid line).
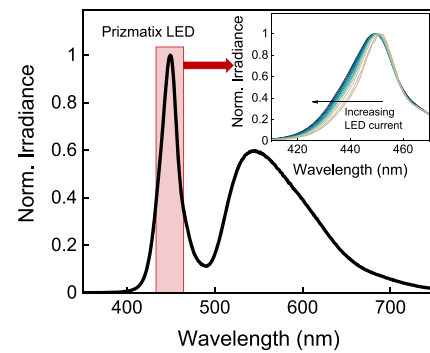

FIG. 2. Normalized laboratory LED source (Prizmatix UHP-T-LED-White) spectrum plotted as a function of wavelength. The inset shows the blueshift seen in the LED emission spectrum at ~450 nm associated with a higher input current.

can then be controlled by selecting the number of "pixels" that are steered toward the DUT or toward baffles.[26]

Varying the radiant power of an LED source

The radiant power of LED sources can be controlled by varying their driving current. However, this will cause a spectral shift in the output spectrum. For most white (e.g., phosphor-coated blue) LEDs, this will manifest primarily as a blueshift and increase in full width at half maximum (FWHM) of the phosphor-related emission peak. Figure 2 shows the emission spectrum of a laboratory LED source (Prizmatix UHP-T-LED-White) plotted as a function of wavelength. The inset shows the corresponding blueshift in emission peak when increasing the LED-driving current. The radiant power of LED sources can be controlled by varying their current, although this approach has limitations in terms of its dynamic range. Operating the LED at extremely low or high currents may not be feasible, which restricts the range of achievable power levels. Typically, pulse-width modulation (PWM) is employed for dimming purposes, but this method is not suitable for accurate and precise testing of indoor photovoltaics (IPV). Therefore, while controlling LED current alone may not be sufficient for IPV testing, it can still be a valuable tool when used in conjunction with other techniques.

Reference devices

Accurate measurement of the spectral irradiance of a light source is a technically challenging task, and comparing the results obtained in different laboratories under varying indoor lighting conditions should be done with great care. Ideally, a spectroradiometer should be used to calibrate the IPV test apparatus, preferably at the location of the device under test (DUT). However, this may not be feasible for all research groups given the different efforts in photovoltaic research and development. In such cases, spectral irradiance can be calculated by separately measuring the spectral shape and total irradiance using equipment commonly found in most research laboratories. The calibration process for this method is discussed in detail in an upcoming work and will be summarized for the purposes of this discussion. In brief, to calibrate an IPV test setup with this method, it is first necessary to measure the total irradiance at the DUT location. For a known light spectrum, this can be achieved by using reference devices with known spectral responsivity, defined as

$$R(\lambda) = \frac{I(\lambda)}{E_e(\lambda)}, \tag{4}$$

where $I(\lambda)$ is the photocurrent of the reference device and $E_e(\lambda)$ denotes the spectral irradiance. The accuracy of calibration depends on the degree of overlap between the incident light spectrum and the spectral responsivity of the reference device. In the context of IPV device calibration, the bandgap of the reference cell/module should be considered, as this will contribute to the uncertainty budget of the test setup. Figure 3(a) shows the spectral responsivity of various commercially available reference cells suitable for this purpose, including a silicon (Si) cell (Thorlabs FDS1010), a Si module (ScienceTech RefQ), a Si photodiode (Newport 818-UV), and a germanium arsenide (GaAs)-based reference cell (Rera), plotted as a function of wavelength. The wavelength-dependent spectral responsivity was measured at three different (wavelength-averaged) light illuminances: ~50, ~200, and ~1000 lx. While the dark-colored lines in Fig. 3(a) correspond to the mean spectral responsivity, the light-colored areas indicate the standard deviation–all four reference devices show no drastic change in spectral responsivity, suggesting sufficient linearity in the selected intensity regime.
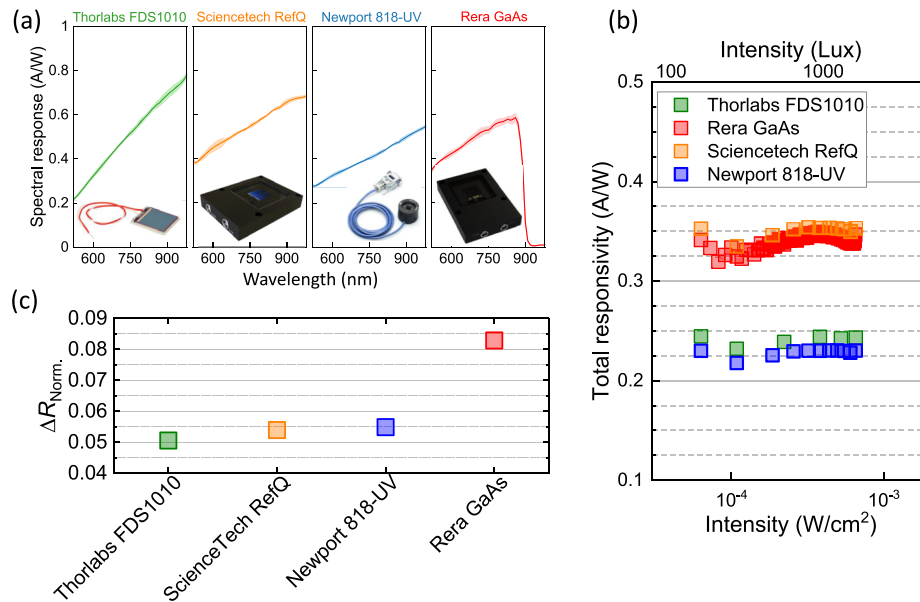
FIG. 3. (a) Spectral responsivity of four reference devices used to calibrate the total irradiance plotted as a function of wavelength: Thorlabs FDS1010 Si cell, ScienceTech RefQ Si module, Newport 818-UV Si photodiode, and Rera GaAs reference cell. The spectral response was measured at three different light intensities: while dark-colored lines are mean responsivity values, light-colored areas indicate the corresponding standard deviation. (b) Total responsivity shown as a function of intensity and compared for all four reference devices. (c) Variation in normalized responsivity (ΔR_{Norm}) of the reference devices when calibrating the IPV test setup as described in the supplementary material. Here, a larger ΔR_{Norm} indicates a greater sensitivity to the attenuator-induced spectral changes in the test setup.

Next, the responsivity of all four reference devices was measured using our IPV test setup, as described in detail in the supplementary material. Here, the 818-UV Si photodiode was used for light intensity calibration, assuming intensity-dependent spectral response and broad wavelength linearity [see Fig. 3(a)]. Figure 3(b) shows the corresponding total (i.e., wavelength-integrated) responsivity as a function of irradiance and is compared for all four reference devices. As shown, all four devices show a non-constant responsivity over the probed intensity regime, indicative of attenuator-induced spectral changes. In this regard, the absolute change in normalized responsivity, as an estimate for attenuator-induced spectral changes, $\Delta R_{Norm} = R_{Norm,max} - R_{Norm,min}$ [see Fig. 3(c)], was determined for all four reference systems, from which the GaAs shows the highest ΔR_{Norm} with ~0.085, as compared to the other three Si-based reference devices: ~0.05 (Thorlabs, FDS1010), ~0.055 (ScienceTech RefQ) and ~0.055 (Newport, 818-UV). We note that attenuator-induced spectral changes of the input light should be in general avoided; the corresponding attenuator can, however, be quite expensive and complex to program.[25] Thus, when using conventional and often spectral change-inducing attenuators, such as ND filters, tandem prisms, or mesh filters, it is recommended to use a reference device for the light intensity calibration process that is sensitive enough to detect those spectral changes (i.e., a reference device with ΔR_{Norm} as large as possible).

Furthermore, the spatial uniformity of the probe light at the position of the reference cell and DUT (preferably the same) needs to be considered. As such, photodiodes with areas significantly smaller than those of the DUT can lead to drastic errors in the estimation of total irradiance if the spatial uniformity is poor. On the other hand, if

bus-barred reference cells are used, it may be challenging to measure their absolute photovoltaic external quantum efficiency (EQE$_{PV}$). In practical terms, it is, therefore, recommended to have good spatial probe beam uniformity and to measure multiple reference devices at the location of the DUT to minimize overall uncertainty. The selection of appropriate reference devices requires attention to attenuator-induced spectral changes, the selection of sensitive reference devices, consideration of spatial probe beam uniformity, and multiple measurements to minimize uncertainty.

Comparison of IPV test setups

To demonstrate the various approaches to broadband attenuation and setup calibration outlined above, an IPV characterization apparatus comprising a 4000 K LED (Prizmatix, UHP-T-LED-White) was built. Figure 4(a) shows a schematic of the IPV test apparatus. To illuminate the device under test (DUT), a liquid light guide (LLD; Prizmatix) was used to transfer the attenuated probe light from the light source (LS) to a collimator (C; Prizmatix) directly attached to a collimation tube (CT). Here, we consider three types of LS attenuation that would be representative of typical equipment available in optoelectronic characterization laboratories, including (i) ND filters mounted onto a motor-controlled wheel with six positions in combination with LED power control, (ii) a tandem prism attenuator (Standa), which is also motor-controlled in combination with LED power control, and finally (iii) the LED only. Note that the LED driver uses an internal PID controller to stabilize the output power.
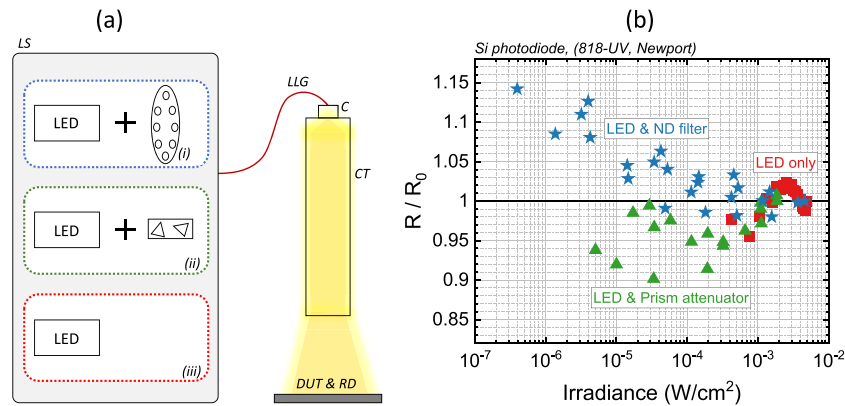
04 November 2024 15:35:14

FIG. 4. (a) Schematic of an IPV test apparatus having different light sources (LSs): (i) LED and neutral density filter wheel; (ii) LED and prism attenuator; and (iii) LED only. (b) Variation in normalized responsivity with varying types of attenuation plotted against the input light intensity.

Figure 4(b) shows the result of the initial calibration with a NIST-calibrated silicon reference photodiode (Newport 818-UV) with known responsivity. For comparison, the normalized responsivity (R/R_0) (calculated via $R = I_{ref}/I_L$, where I_{ref} denotes the reference photodiode current and I_L denotes the input light intensity) points are plotted against the light intensity. As the only form of attenuation, the range of irradiances achievable by varying the LED output power (blue symbols) is only one order of magnitude (i.e., $\sim 10^{-3} < I_L < 10^{-2}$ W/cm^2), thus much smaller in comparison to the prism coupler (green symbols) (about 2 orders of magnitude; $\sim 10^{-5} < I_L < 10^{-3}$ W/cm^2) and ND filter (red symbols) (four orders of magnitude; $\sim 10^{-6} < I_L < 10^{-2}$ W/cm^2). Despite the increased irradiance window available to probe the photovoltaic performance under indoor illumination, the ND filter wheel attenuation contributes the largest source of spectral-induced error with a maximum change of responsivity of up to 15%. In comparison, attenuation induced responsivity changes, when using the LED only, are minimized to ~3% only. As mentioned above, lower irradiances can also be achieved with the LED power control alone, e.g., by increasing the distance between the collimation tube and the DUT. However, this approach may require a lot of space and thus have limited practicality.

Uncertainty and spectral deviation

Changes in the spectral shape of indoor light broadband sources will inevitably influence the accuracy of light intensity calibration and the performance characterization of IPV devices. To this end, we simulated the indoor PCE intensity dependence of a ~500 nm tick, 1.79 eV bandgap $FA_{0.85}Cs_{0.15}Pb(I_{0.6}Br_{0.4})_3$ perovskite PV device, comparing different degrees of attenuator-induced changes in the spectral shape of a broadband light source. Details of the perovskite device fabrication and performance characterization under AM1.5 G conditions are provided elsewhere.[27] For the simulations, we used a recently introduced approach, which estimates realistic limits for PCEs under any input spectrum while accounting for radiative and non-radiative losses.[28]

In our calculations, we compared the above three IPV test setups with indoor light attenuation via (i) LED power control only, (ii) prism attenuator, and (iii) ND filters. The corresponding light spectra at different light attenuation settings were recorded manually using a photonic multichannel analyzer (PMA-12, Hamamatsu) and used as input spectra. The recorded spectra are shown in the supplementary material, Fig. S1. Figures 5(a)–5(c) show the relative changes in output spectra (I/I_o) for the three IPV apparatus setups. Here, only minor changes are observed for light attenuation via LED power control only [see Fig. 5(a)], characterized by $I/I_o \approx 1$ across the wavelength regime. Minor changes at ~450 nm are caused by the shift in the LED emission spectrum associated with a change in input current. The prism attenuator, on the other hand, clearly affects the shape of the broadband LED spectrum for wavelengths >500 nm—a maximum $I/I_o \approx 2$ is observed for the strongest attenuation [see Fig. 5(b)]. Finally, as shown in Fig. 5(c), light attenuation via ND filters causes drastic changes in the shape of the output spectrum. In particular, the transmission of high wavelengths (i.e., >650 nm) increases at higher attenuations, noticeably disturbing the shape of the broadband LED spectrum ($I/I_o > 10$).

Figures 5(d)–5(f) show the relative change in responsivity vs irradiance of the perovskite device, as expected for different IPV test setups, and attenuator-induced changes in corresponding input spectra shape [see Figs. 5(a)–5(c)] with respect to the CIE-LED-B4 standard spectrum at 1000 lx [black, dashed lines in Figs. 5(d)–5(f)]. The responsivity was hereby calculated as $R = I_{sc}/P_{in}$ (where I_{sc} denotes the device short-circuit current and P_{in} defines the incident light power) using the methodology outlined in detail in Ref. 28. The black, dashed lines in Figs. 5(d)–5(f) correspond to the normalized responsivity, as expected for the CIE-LED-B4 standard spectrum at 1000 lx. It becomes clear that changes in input spectrum shape, i.e., both (i) spectrum changes associated with a certain light source and (ii) attenuated-induced spectrum shape changes, are inevitably linked to a change in responsivity. As shown in Figs. 5(d)–5(f), (i) and (ii) combined can lead to responsivity changes (δ_R) of up to ~2% (LED power control only), ~6% (prism attenuator), and ~15% (ND filter wheel) for our Prizmatix LED. Those responsivity changes are expected to be ultimately reflected in
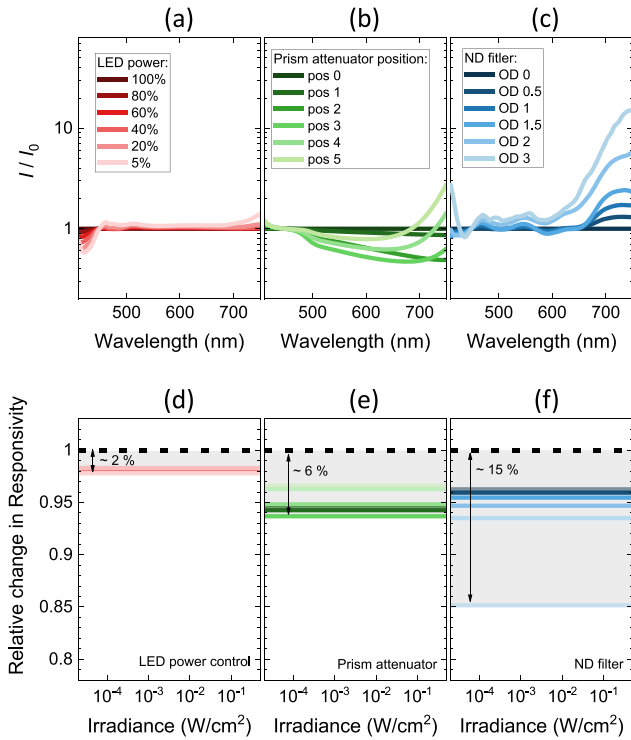
FIG. 5. Relative change in output spectrum plotted as a function of wavelength and comparing different light attenuation via (a) LED power control, (b) prism attenuator, and (c) neutral density filter wheel. Relative change in responsivity, as expected for indoor light attenuation with (d) LED power control, (e) prism attenuator, and (f) ND filters, and attenuator-induced changes in corresponding input spectra [see Figs. 5(a)–5(c)] with respect to the CIE-LED-B4 standard spectrum at 1000 lx (black, dashed lines). The responsivities were calculated for a wide-gap perovskite device (Ref. 27) along (Ref. 28).

the PCE, given that $PCE = V_{oc}I_{sc}FF/P_{in} = RV_{oc}FF$, thus $\delta_{PCE} \propto \delta_R$ (see the supplementary material, Fig. S1). It becomes clear that among the three tested attenuation systems, broadband light attenuation via LED only leads to the lowest errors—the same result was found for a silicon- and GaAs-based reference device (see Fig. S2 in the supplementary material). We note, however, that those spectral changes can, in general, be accounted for. As such, one can determine the so-called spectral deviation (*SPD*) of any IPV test apparatus,

$$SPD = \left(\frac{\sum |E_{SIM}(\lambda) - E_{ref}(\lambda)| \times \Delta\lambda}{\sum E_{ref}(\lambda) \times \Delta\lambda} \right) \times 100\%, \quad (5)$$

where $E_{ref}(\lambda)$ denotes the reference spectrum (given the lack of a defined standard indoor spectrum at the moment of writing, the CIE standard illuminant LED-B4 spectrum is most convenient to use), and $E_{SIM}(\lambda)$ refers to the spectrum of the IPV test apparatus light source. A spectral deviation of ~27% is calculated for the Prizmatix LED, as used in our IPV test apparatus, compared to the CIE LED-B4 standard.

Finally, we want to emphasize that one can, in principle, also correct for spectral changes induced through the IPV attenuator system using a correction function. However, doing so in a dynamic way (i.e., measuring at different light intensities) necessarily increases the uncertainty of the measurement. As such, the propagation of the measurement uncertainty of (i) the spectrum at each attenuator condition and (ii) the additional uncertainty in returning to that specific condition would increase.

In practical terms, it is, therefore, recommended to use an IPV test apparatus with light attenuation characterized by as few changes in spectral shape as possible. In particular, the high wavelength regimes are expected to contribute to the spectrum at high light attenuation when using conventional prism and ND filter attenuators [see Figs. 5(b) and 5(c)]. For light attenuation in an IPV test apparatus (additionally) controlled via LED power control, one needs to consider changes in the low wavelength regime as associated with the LED pump peak emission [see Fig. 5(a)]. Both, spectral deviations of the IPV test apparatus light source to a standard (e.g., CIE LED-B4) and attenuator-induced spectral changes must be considered when probing PV figures of merit.

CONCLUSIONS

With the convergence of advancements in low-power electronics, wireless communications, automation, big data, and sensors, the emergence of ambient light harvesting via indoor photovoltaics is set to create fresh prospects in areas such as wireless sensing and the Internet of Things (IoT). To enable the growth of this field, accurate characterization methods for IPV devices are required. Measuring IPV devices over a broad irradiance range provides both practical and theoretical insights that will prove invaluable in scientific and technical development. The spectral dependence of the attenuator systems used to reproducibly create varying irradiance can lead to sources of uncertainty if not properly considered. Further, suitable reference devices with good linearity should be used that are optimal for the light source and bandgap of the PV system being characterized. Here, reference devices that are sensitive to spectral changes (i.e., large ΔR_{Norm}) are recommended. The origin of spectral changes in the output spectrum can be, *inter alia*, related to LED-driving current variations and attenuator-induced wavelength transmission changes. For our IPV test apparatus, we determined those non-linear phenomena to cause uncertainty in responsivity (and, thus, power conversion efficiency) as high as ~15% when using conventional ND filters.

SUPPLEMENTARY MATERIAL

The derivation of the expression for spatial non-uniformity, a description of the calibration procedure, and data obtained under additional experimental conditions are given in the supplementary material.

ACKNOWLEDGMENTS

AUTHOR DECLARATIONS

Conflict of Interest

The authors have no conflicts of disclose.

Author Contributions

S.Z. performed the experiments. P.M. and A.A. assisted with analyzing and interpreting the data. G.B. supervised the work. All authors contributed to development of the manuscript first drafted by S.Z. together with G.B.

Stefan Zeiske: Conceptualization (equal); Data curation (equal); Formal analysis (equal); Investigation (equal); Methodology (equal); Project administration (equal); Software (lead); Supervision (equal); Validation (equal); Visualization (equal); Writing – original draft (equal); Writing – review & editing (equal). **Paul Meredith**: Conceptualization (equal); Data curation (equal); Formal analysis (equal); Funding acquisition (equal); Investigation (supporting); Methodology (supporting); Project administration (equal); Resources (equal); Software (lead); Supervision (equal); Validation (equal); Visualization (equal); Writing – original draft (equal); Writing – review & editing (equal). **Ardalan Armin**: Conceptualization (equal); Formal analysis (equal); Funding acquisition (equal); Investigation (equal); Methodology (equal); Project administration (equal); Resources (equal); Supervision (equal); Validation (equal); Writing – review & editing (equal). **Gregory Burwell**: Conceptualization (equal); Data curation (equal); Formal analysis (equal); Funding acquisition (equal); Investigation (equal); Methodology (equal); Project administration (equal); Resources (equal); Supervision (equal); Validation (equal); Visualization (equal); Writing – original draft (lead); Writing – review & editing (equal).

DATA AVAILABILITY

The data that support the findings of this study are available within the supplementary material.

REFERENCES

[1] H. S. Ryu, S. Y. Park, T. H. Lee, J. Y. Kim, and H. Y. Woo, "Recent progress in indoor organic photovoltaics," Nanoscale **12**(10), 5792–5804 (2020).

[2] K.-L. Wang, Y.-H. Zhou, Y.-H. Lou, and Z.-K. Wang, "Perovskite indoor photovoltaics: Opportunity and challenges," Chem. Sci. **12**(36), 11936–11954 (2021).

[3] M. Freitag, J. Teuscher, Y. Saygili *et al.*, "Dye-sensitized solar cells for efficient power generation under ambient lighting," Nature Photon **11**, 372–378 (2017).

[4] H. K. H. Lee, J. Barbé, and W. C. Tsoi, *Solar Cells and Light Management: Materials, Strategies and Sustainability* (Elsevier, 2019), pp. 355–388.

[5] I. Mathews, S. N. Kantareddy, T. Buonassisi, and I. M. Peters, "Technology and market perspective for indoor photovoltaic cells," Joule **3**(6), 1415–1426 (2019).

[6] M. A. Iqbal, H. Sajjad, H. Xing, and M. A. Imran, *Enabling the Internet of Things Fundamentals, Design, and Applications* (Wiley, 2021).

[7] C. Polyzoidis, K. Rogdakis, and E. Kymakis, "Indoor perovskite photovoltaics for the Internet of things—Challenges and opportunities toward market uptake," Adv. Energy Mater. **11**(38), 2101854 (2021).

[8] X. Hou, Y. Wang, H. K. H. Lee, R. Datt, N. Uslar Miano, D. Yan, M. Li, F. Zhu, B. Hou, W. C. Tsoi, and Z. Li, "Indoor application of emerging photovoltaics—Progress, challenges and perspectives," J. Mater. Chem. A **8**(41), 21503–21525 (2020).

[9] B. Li, B. Hou, and G. A. J. Amaratunga, "Indoor photovoltaics, *The Next Big Trend* in solution-processed solar cells," InfoMat **3**(5), 445–459 (2021).

[10] M. Li, F. Igbari, Z. K. Wang, and L. S. Liao, "Indoor thin-film photovoltaics: Progress and challenges," Adv. Energy Mater. **10**(28), 2000641 (2020).

[11] M. Mainville and M. Leclerc, "Recent progress on indoor organic photovoltaics: From molecular design to production scale," ACS Energy Lett. **5**(4), 1186–1197 (2020).

[12] O. Almora, D. Baran, G. C. Bazan, C. I. Cabrera, S. Erten-Ela, K. Forberich, F. Guo, J. Hauch, A. W. Y. Ho-Baillie, T. J. Jacobsson, R. A. J. Janssen, T. Kirchartz, N. Kopidakis, M. A. Loi, R. R. Lunt, X. Mathew, M. D. McGehee, J. Min, D. B. Mitzi, M. K. Nazeeruddin, J. Nelson, A. F. Nogueira, U. W. Paetzold, B. P. Rand, U. Rau, H. J. Snaith, E. Unger, L. Vaillant-Roca, C. Yang, H.-L. Yip, and C. J. Brabec, "Device performance of emerging photovoltaic materials (version 3)," Adv. Energy Mater. **13**, 2203313 (2023).

[13] L. K. Jagadamma and S. Wang, "Wide-bandgap halide perovskites for indoor photovoltaics," Front. Chem. **9**, 632021 (2021).

[14] G. Burwell, O. J. Sandberg, W. Li, P. Meredith, M. Carnie, and A. Armin, "Scaling considerations for organic photovoltaics for indoor applications," Sol. RRL **6**(7), 2200315 (2022).

[15] D. Lü, P. Hartnagel, M. H. Lsbeck, and T. Kirchartz, "Understanding the thickness and light-intensity dependent performance of green-solvent processed organic solar cells," ACS Mater. Au **3**, 215 (2023).

[16] S. K. Thomas, A. Pockett, K. Seunarine, M. Spence, D. Raptis, S. Meroni, T. Watson, M. Jones, and M. J. Carnie, "Will the internet of things be perovskite powered? Energy yield measurement and real-world performance of perovskite solar cells in ambient light conditions," IoT **3**(1), 109–121 (2022).

[17] Y. Cui, L. Hong, T. Zhang, H. Meng, H. Yan, F. Gao, and J. Hou, "Accurate photovoltaic measurement of organic cells for indoor applications," Joule **5**(5), 1016–1023 (2021).

[18] D. Lübke, P. Hartnagel, J. Angona, and T. Kirchartz, "Comparing and quantifying indoor performance of organic solar cells," Adv. Energy Mater. **11**(34), 2101474 (2021).

[19] N. Talbanova, T. Komaricheva, L. O. Luchnikov, G. Ermolaev, V. Kurichenko, D. S. Muratov, A. Arsenin, I. S. Didenko, V. Volkov, I. V. Badurin, M. V. Ryabtseva, N. T. Vagapova, D. Saranin, and A. Di Carlo, "Color-temperature performance of perovskite solar cells under indoor illumination," Sol. Energy Mater. Sol. Cells **254**, 112284 (2023).

[20] S. Zeiske, W. Li, P. Meredith, A. Armin, and O. J. Sandberg, "Light intensity dependence of the photocurrent in organic photovoltaic devices," Cell Rep. Phys. Sci. **3**(10), 101096 (2022).

[21] S. Beuel, P. Hartnagel, and T. Kirchartz, "The influence of photo-induced space charge and energetic disorder on the indoor and outdoor performance of organic solar cells," Adv. Theory Simul. **4**(3), 2000319 (2021).

[22] M. Stolterfoht, A. Armin, B. Philippa, and D. Neher, "The role of space charge effects on the competition between recombination and extraction in solar cells with low-mobility photoactive layers," J. Phys. Chem. Lett. **7**(22), 4716–4721 (2016).

[23] S. Zeiske, O. J. Sandberg, N. Zarrabi, W. Li, P. Meredith, and A. Armin, "Direct observation of trap-assisted recombination in organic photovoltaic devices," Nat. Commun. **12**(1), 3603 (2021).

[24] N. Zarrabi, O. J. Sandberg, S. Zeiske, W. Li, D. B. Riley, P. Meredith, and A. Armin, "Charge-generating mid-gap trap states define the thermodynamic limit of organic photovoltaic devices," Nat. Commun. **11**, 5567 (2020).

[25] G. Koutsourakis, T. Eales, I. Kroeger, and J. C. Blakesley, "High-resolution linearity measurements of photovoltaic devices using digital light processing projection," Meas. Sci. Technol. **32**, 055901 (2021).

[26] F. Bausi, G. Koutsourakis, J. C. Blakesley, and F. A. Castro, "High-speed digital light source photocurrent mapping system," Meas. Sci. Technol. **30**(9), 095902 (2019).

[27] P. Caprioglio, J. A. Smith, R. D. J. Oliver, A. Dasgupta, S. Choudhary, M. D. Farrar, A. J. Ramadan, Y.-H. Lin, M. G. Christoforo, J. M. Ball, J. Diekmann, J. Thiesbrummel, K.-A. Zaininger, X. Shen, M. B. Johnston, D. Neher, M. Stolterfoht, and H. J. Snaith, "Open-circuit and short-circuit loss management in wide-gap perovskite p-i-n solar cells," Nat. Commun. **14**, 932 (2023).

[28] A. M. Kay, M. Fitzsimons, G. Burwell, P. Meredith, A. Armin, and O. J. Sandberg, "The thermodynamic limit of indoor photovoltaics based on energetically-disordered molecular semiconductors," Sol. RRL 2300277 (2023).

04 November 2024 15:35:14